Applied Thermal Engineering 137 (2018) 268–276

Contents lists available at ScienceDirect

Applied Thermal Engineering

journal homepage: www.elsevier.com/locate/apthermeng

Research Paper

Pool-boiling enhancement using multilevel modulated wick

Yahya Nasersharifi[a], Massoud Kaviany[b], Gisuk Hwang[a,*]

[a] Department of Mechanical Engineering, Wichita State University, Wichita, KS 67260, United States
[b] Department of Mechanical Engineering, University of Michigan, Ann Arbor, MI 48109, United States

HIGHLIGHTS

- Controlled hydrodynamic instability wavelength enhances Critical Heat Flux (CHF).
- Thin monolayer wick significantly Heat Transfer Coefficient (HTC).
- The novel 3D wick structures simultaneously enhances CHF and HTC.

ARTICLE INFO

Keywords:
Phase separation
Sintered particles
Wick superheat

ABSTRACT

Main challenges in saturated pool-boiling heat transfer are limited Critical Heat Flux (CHF) and Heat Transfer Coefficient (HTC), caused by the counterflow of liquid and vapor over the heated surface. Using multilevel modulated wicks, i.e., monolayer, columnar, and mushroom post wicks, we control the liquid and vapor flow for efficient phase separation, thereby improving the CHF and HTC. The wicks are fabricated using multi-step sintering process using 200 μm copper particles, and the pool boiling uses *n*-pentane at ambient pressure. The monolayer wicks without and with the mushroom post structure provide 20% and 87% CHF enhancements, respectively, compared to the plain surface. It is found that the CHF enhancement of the mushroom wick is attributed to its pitch distance, 3.5 mm, which effectively reduce the hydrodynamic instability (Rayleigh-Taylor) wavelength. The further reduction of the pitch distance, 1 mm, results in the 250% CHF improvement in agreement with the theory. The columnar and mushroom posts with monolayer increase HTC by tenfold, compared to the plain surface, due to the reduced conduction path through the thin monolayer wick under the controlled vapor region using the columnar and mushroom post wick (vapor chamber-like environment in pool boiling). The multilevel wick design provides fundamental insights into simultaneous CHF and HTC enhancements with potential use in advanced thermal management systems.

1. Introduction

A pool boiling offers a passive high heat flux cooling technology with a minimal temperature gradient for various applications including miniaturized electronic cooling [1–4], renewable energy system [5], and safe operations in energy production [6]. However, main technical challenges are a limited heat removal capability, so called, Critical Heat Flux (CHF), and a poor Heat Transfer Coefficient (HTC) due to a premature surface dryout. On a plain surface, the surface dryout is related to a poor liquid supply to an evaporator, limited by critical liquid-vapor hydrodynamic wavelength, i.e., Rayleigh-Taylor instability wavelength. For an infinitely-large plain surface, the CHF, $q_{CHF,Z}$, is predicted by the following relation [7],

$$q_{CHF,Z} = \frac{\pi}{24}\rho_g^{1/2}\Delta h_{lg}[\sigma g(\rho_l - \rho_g)]^{1/4}. \quad (1)$$

where ρ_g and ρ_l are the vapor and liquid densities, respectively, Δh_{lg} is the heat of evaporation, σ is the surface tension. This limiting pool-boiling performance has motivated much research efforts to understand the dryout mechanisms and enhance the CHF and HTC. Various micro-/nanoscale surface engineering approaches have shown CHF and/or HTC enhancements by improving the liquid supply to the evaporator (or vapor escape from the evaporator) including rough surfaces [8–12], random porous matrices [13], microchannels/grooves [14,15], foams [16–18], mesh-like wicks [19], uniform porous coatings [20–24], nanostructures [25,26], and hybrid micro-/nanostructures [27–29].

One early approach is to employ uniformly thick microporous structures [30,31]. Nishikawa et al. (1979) have employed uniform sintered particles to examine the effects of coating thickness in a tube surface on the CHF and HTC, and reported that ~1 mm thickness is the optimal thickness [32]. Oconnor and You (1995) and Chang and You

* Corresponding author.
E-mail address: Gisuk.Hwang@wichita.edu (G. Hwang).

https://doi.org/10.1016/j.applthermaleng.2018.03.073
Received 1 September 2017; Received in revised form 12 February 2018; Accepted 21 March 2018
Available online 22 March 2018
1359-4311/

Nomenclature

g	gravitational acceleration (m/s^2)
Δh_{lg}	enthalpy of vaporization (J/kg)
k	thermal conductivity (W/m K)
l	separation distance (m)
p	pressure (Pa)
q	heat flux (W/m^2)
r	pore or meniscus radius
T	temperature (°C)
u	velocity (m/s)
U	uncertainty

Greek symbols

δ	wick thickness (m)
λ	instability wavelength (m)
ρ	density (kg/m^3)
σ	surface tension (N/m)

Subscripts

c	capillary, or critical
CHF	critical heat flux
g	gas
l	liquid
lg	phase change, or saturation
m	modulated
p	plain surface, particle, prediction, post, or pitch
R	Rohsenow
RT	Rayleigh-Taylor
s	surface
u	uniform
w	wick
Z	Zuber

(1997) have studied that a microporous coating enhanced both the CHF and HTC in a pool boiling, and concluded that the enhancements are related to the increased active nucleation site density from the direct visualizations [20,33]. Borzenko and Malyshenko (2001) have examined the dryout mechanisms in porous coating by measuring the surface temperature to further understand the CHF and HTC enhancement mechanisms [34]. Kim and You (2002) have also articulated that the increased active nucleation site density, decreased the bubble size, and increased departure frequency for increased convection heat transfer and/or favorable hydrodynamic instability changes [35]. Hwang and Kaviany (2006) have examined that the various uniform microporous coatings using sintered copper particles with different particle sizes and different types of copper particles on the pool boiling performance using *n*-pentane, showing doubled CHF with significant HTC improvements [23]. They have concluded that the CHF enhancement of the uniform microporous coatings is attributed to the reduced hydrodynamic instability wavelength, while the different types of particles could change HTC. Choon et al. (2006) have investigated that the pool boiling enhancement using a uniform metallic foam at subatmospheric pressure, i.e., 1.8 kPa, and the enhanced HTC has been explained using the modified Rohsenow correlation [16]. Li and Peterson (2006) have studied the effects of the wire diameter, porosity, and thickness of the sintered copper mesh on the enhanced CHF and HCT using water [36,37], including the different vapor escape mode depending on the different aspect ratio of the heater size to porous layer thickness [38]. Launay et al. (2006) have fabricated Si micropillar structures coated with carbon nanotube (CNT) to enhance the pool boiling performance using PF5060 and water as working fluids [39]. They have found that the CNT enables to increase the HTC, especially at the low superheat region. Furbeg and Palm (2011) have used foam structures (dendrite micro structures) and visualized that the bubble departure frequency increases using R-134a and FC-72, due to the increased evaporation sites, and this in turn results in the HTC improvement [40]. Pialago et al. (2013) have also developed a cold spray Cu-CNT composite coating technique and apply it to the pool boiling performance enhancement using R-134a [41]. This surface improves the CHF up to 74% with moderate superheat reduction. Similarly, Zheng and Park (2015) have also employed the ball-milled Cu-composite coatings on the pool boiling performance enhancement [28]. Kim et al. (2015) have reported the effects of the different coolants (R-123 and water) on the CHF and HTC in the pool boiling using uniform microporous coatings [22]. Xu and Zhao (2016) have examined gradient metal foam to control the desired bubble morphology and mitigate the large fluid resistance property by controlling foam density [42]. Recently, Gheitaghy et al. (2017) have employed the electrodeposition method for the uniform Cu microstructure to enhance the pool boiling performance, and this results in the 60% CHF enhancement with 200% HTC improvement [24]. Sun et al. (2017) have used the microgrooves with reentry cavities, aiming at increasing HTC and early onset of nucleate on the pool boiling [43].

The micro-machined surfaces have also shown the CHF and HTC enhancements. Kim and Choi (2001) have used machined micro porous structures on tube to enhance the pool boiling performance up to 6.5 times compared to the plain surface using R-11, R-123, and R-134a [44]. Das et al. (2009) have studied the effects of the microchannels on the pool boiling by increasing the evaporation areas, and this results in the heat flux enhancement up to 250 W/cm^2 using water [14]. Cooke and Kandlikar (2012) has examined the CHF and HTC enhancement in the pool boiling using the open microchannels (200–400 μm) and water, showing 244 W/cm^2 (maximum heat flux without reaching CHF) with a 26.9 W/cm^2 K [45]. This enhancements are related to early bubble nucleation, larger bubble departure diameters, improved HTC from larger vapor generation rate in presence of extended heated surface area [45,46]. Kruse et al. (2015) have employed femtosecond laser to fabricate the mound-like microstructure coated with the nanostructures in stainless-steel surface to enhance CHF and HTC using water [47]. They have concluded that the enhancements are related to improved wicking and wettability. Jaikumar and Kandlikar (2016) has employed the microchannels (300–762 μm) coated with the sintered particles (fin top, channels only, and entire fin surfaces) to understand the effects of the controlled liquid supply and bubble escape mechanism on the CHF and HTC [48]. This study has shown the enhanced CHF up to 420 W/cm^2 over 1 cm^2 with 1.7 °C using fin top sintered particles. Dhillon et al. (2015) has examined the micropillar structures with the nanopillars on the CHF enhancement mechanism, using the direct bubble morphology and local temperature distributions. It concludes that this CHF mechanism is related to the improved rewetting time in presence of the micropillar structures [49].

To further improve the pool boiling performance, nonuniform surface engineering approaches have been also employed, and the thorough literature reviews are found in the previous work [50]. Liter and Kaviany (2001) have employed the 3D conical wick structure to control the dominant bubble nucleate sites through the thin wick, and critical hydrodynamic instability wavelength using the pitch distance of the thick wick, showing that the CHF is 3 times higher compared to the plain surfaces [51]. Min et al (2009) have also employed 2D modulated microporous structures with grooves to similarly mitigate the hydrodynamic instability by reducing the critical hydrodynamic instability wavelength [52]. Li and Peterson (2010) have also demonstrated that the 3D porous post structures could improve the HTC and CHF using

water [53]. Xu et al. (2011) have utilized metallic foams with V-shape groove to enhance the bubble escape from the heated surface, aiming at enhancing the HTC and CHF in pool boiling with water [54]. Qu et al. (2012) have employed metallic foam with V-shape grooved on the enhanced pool-boiling experiment using saturated water [55], and they have concluded that the enhancement is related to the combinations of reduced bubble escaping resistance, improved evaporation surface area, and capillary-driven liquid supply assisted by the V-shape groove. Patil and Kandlikar (2014) [15] and Jaikumar and Kandlikar (2015) have developed open microchannels coated with porous fin tops to improve the liquid-vapor phase separation for the enhanced CHF up to 3.3 times compared to the plain surface using water [56]. Bai et al (2016) have developed a 3D hybrid structure, i.e., channels combined uniform sintered particles, to improve the liquid-vapor phase separation for enhanced pool boiling performance [57]. This results in the enhanced CHF of 416 W/cm^2 using water as a working fluid. Tang et al (2016) have also studied the similar 2D modulated structures using copper particles with different morphology, particle size, and modulated structures [58]. The pool boiling performance maximizes with the copper particle sizes of 50–75 μm using water. Also, the nonuniform (distributed) surface coatings have shown to simultaneously increase the CHF and improved the HTC in heat pipes [59], vapor chambers [60–64], and flow boiling [65], by assisting the liquid supply to the heated surface using rather thick capillary structures.

Previous studies have shown that the nonuniform microstructures effectively improves the CHF and HTC compared to uniform microstructure, by precisely controlling the critical hydrodynamic instability wavelength using the thick wick, i.e., enhanced CHF, and reducing the effective conduction pathway using the thin wick, i.e., improved HTC [51,52]. Recent studies show that the monolayer wick (single layer of sintered copper particles) combined with such 3-D wick structures result in very high HTC, i.e., 200,000 W/m^2 K with enhanced CHF up to 6 times compared to the plain surface pool boiling CHF using water [61,62]. Although these novel wick designs (monolayer wick combined with 3-D capillary structure) show significant advancements of CHF and HTC, comprehensive understanding of multilevel wick design for pool boiling has not been fully realized yet. Here, we examine the multilevel micro-structure modifications for CHF and HTC enhancements using novel 3-D sintered-particle wick structures namely, monolayer, columnar, mushroom posts wicks, with the aim of active control of the hydrodynamic instability wavelength and use of the monolayer wick to improve the HTC.

2. Multi-level modulated wicks

To simultaneously enhance the CHF and HTC, we design multi-level modulated wicks, namely, monolayer (Design B), columnar posts (Design C), and mushroom posts (Design D), using sintered spherical particles as shown in Fig. 1. To examine their pool boiling heat transfer, the heat flux is measured as a function of the wick superheat, until CHF, and the pool boiling performances of the wick structures are compared to the plain surface (Design A). The key parameters in pool-boiling heat transfer are (i) reduced Rayleigh-Taylor instability wavelength, λ_m through the capillary body for enhanced CHF, and (ii) reduced effective wick thickness for the large HTC. The detailed descriptions are given below.

2.1. Monolayer (Design B)

The monolayer wick is a single layer of the copper sintered particles of diameter of 200 μm. The multiple-layer wick using the spherical particles (or powders) have been explored in pool boiling, concluding that the optimal number of layer is approximately 3–4, primarily due to the effective bubble generation near surface, thermal-hydraulic wavelength modulation, and/or increased bubble departure frequencies [23,33,66–70]. Here, the monolayer wick is employed to primarily increase the HTC by decreasing effective wick thickness. In fact, the effective HTC is also particle size dependent via the effective thermal conductivity [61], here we focus on the role of the monolayer wick assisted by the columnar and mushroom posts wicks without changing the particle size.

2.2. Columnar posts (Design C)

The columnar posts wick is employed by adding thick columnar posts to the monolayer wick to actively control (or reduce) the Rayleigh-Taylor instability wavelength through the pitch distance between adjacent columnar posts, for significant CHF and HTC enhancement [51,52].

The primary purpose of the thick columnar wick is to assist the liquid supply from the liquid pool via capillary flow, while the thin monolayer wick is used for a HTC enhancement by reduced conduction resistance to evaporation sites, i.e., tips of the capillary meniscus on the monolayer wick. Since the active evaporation sites are located in the liquid meniscus of the monolayer, the vapor generates and escapes from the spacings among the columns. This in turn results in a prescribed liquid-vapor phase separation, thereby leading to the active control of

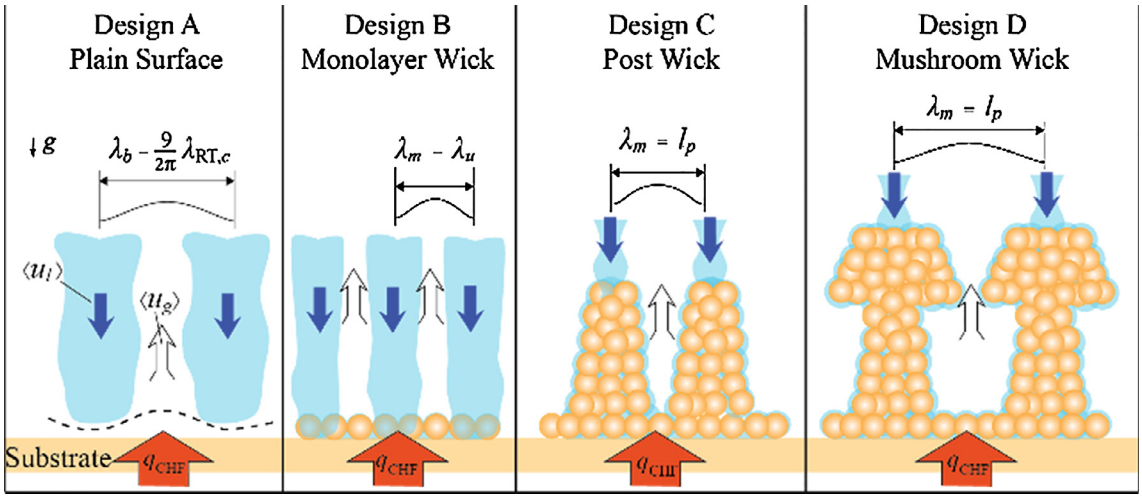

Fig. 1. Schematic drawing of multi-level modulated wick in pool boiling, including the plain surface (Design A), monolayer (Design B), columnar posts (Design C), and mushroom posts (Design D) wicks. The heat flux, wick geometries, liquid/vapor flows, hydrodynamic instability wavelengths are also shown.

the hydrodynamic instability wavelength, λ_m, i.e., Rayleigh-Taylor instability wavelength. The column pitch actively controls (or modulates) the hydrodynamic instability wavelength, with $l_p = \lambda_m$, and the q_{CHF} as predicted in [51]

$$\frac{q_{CHF}}{\frac{\pi}{24}\rho_g^{1/2}\Delta h_{lg}[\sigma g(\rho_l-\rho_g)]^{1/4}} = \frac{3\left[\frac{\sigma}{g(\rho_l-\rho_g)}\right]^{1/4}}{\lambda_m^{1/2}}. \quad (2)$$

The columnar posts wick needs larger particle size than the monolayer wick for larger permeability for minimal viscous pressure drop [61,62], but here the same particles were used for easy fabrication.

2.3. Mushroom posts (Design D)

To further increase the HTC, the mushroom cap structure is added (Design D) in Fig. 1. The mushroom posts allow for easier supply of liquid to the monolayer due to the extra surface area provided by the caps, and this can in turn allow for delayed surface dryout. The mushroom caps also prevent from immediate vapor leaving, which in turn promotes the evaporation near the monolayer wick, i.e., increased HTC, especially in the high heat flux regime.

3. Experiment

3.1. Sample preparations: plan surface and wick fabrications

Plain surface: the plain surface was prepared using a copper rod with a diameter of 3.91 cm. The copper surface was polished using fine sandpapers (P6000 Grit) and the surface was cleaned using alcohol afterward. This polished surface was immediately installed in the test setup, to measure the boiling heat transfer of the polished surface (non-oxidized surface). Also, to test the oxidized copper surface, the polished surface was placed in the laboratory at ambient condition for one week.

Monolayer: the monolayer wick (Fig. 1, B), was fabricated using a commercially-available, thin copper disk with a diameter of 3.81 cm and a thickness of 0.8 mm was used as a substrate, as shown in Fig. 2. The one layer of copper particles with a diameter of 200 μm was uniformly spread over the copper disk, while carefully controlling the number of layer. This particle-covered sample was placed in a furnace under Ar gas flow with 50 sccm for two hours at 950 °C. The monolayer sample was naturally cooled down to the ambient temperature with the cooling rate of 5–10 °C per min. The top view of the fabricated monolayer wick is shown in Fig. 2(d).

Columnar posts: these wicks were made of the monolayer and columnar posts wicks. To carefully control the height of the columnar posts wick and distance among the columnar posts pitch, l_p, a mold was designed and manufactured. The detailed fabrication steps were illustrated in Fig. 3(a) to (c). The stainless steel mold was used to shape the copper particles to the desired geometry and posts pitch during the sintering process. For uniform pitch distances among the columns, the mold was designed to have a hexagonal cell pattern. First, the posts copper particles with d_p = 200 μm were poured in the mold [Fig. 3(a)]. The mold holes were machined in conical shape with 10° inclination, which enabled ease of release from the structure. To ensure close packing, the filled mold was well shaken before the sintering. A monolayer of copper particles with d_p = 200 μm was covered on top of the mold top surface [Fig. 3(b)]. The mold was designed to allow only for one layer of copper particles on the top. The particle-filled mold was placed in furnace under inert gas for two hours at 950 °C [Fig. 3(c)], followed by natural cooling at 5–10 °C/min. The pitch distance, l_p, is controlled for the hydrodynamic instability wavelength [51,52], and we used l_p = 3.5 and 1 mm. The individual post has a columnar structure with the diameter of 2.5 mm and height of 2 mm, and the fabricated columnar posts wick is shown in Fig. 3(d).

Mushroom posts: the mushroom posts wick with the monolayer wick (Fig. 1, Design D), was fabricated in a two-step sintering process utilizing copper particles. For the first two steps, we repeated the fabrication processes of Fig. 3(a) to (c), with additional step to fabricate the mushroom cap as shown in Fig. 4(a) to (c). To add the mushroom caps to the columnar structure, the copper particles poured into the second home-made mold [Fig. 4(a)], and the upside-down columnar posts wick was placed and pressed to ensure the contact between them [Fig. 4(b)]. The entire structure was placed in the furnace under Ar gas for another two hours at 950 °C, followed natural cooling at a rate of 5–10 °C/min. The mold was carefully removed to release the mushroom posts wick without physical damage [Fig. 4(c)]. The fabricated mushroom posts wick is also shown in Fig. 4(d).

3.2. Pool-boiling setup/measurement

The pool-boiling test setup, measurement procedures, and data reduction are based on the previous work [71] as shown in Fig. 5. The setup consists of evaporator, condenser, and adiabatic sections in between. Eight identical cartridge heaters were inserted into the cylindrical copper base to have 2 kW, which provided large enough heating power to reach CHF. The evaporator wicks were placed at the top of the copper base for the pool-boiling experiments. A thermal paste, OMEGATHERM™ 201 (thermal conductivity of $k \sim 2.3$ W/m K) from Omega Engineering, Inc., was applied at the interfaces between the copper base/sample and the sample/main heater block to reduce the

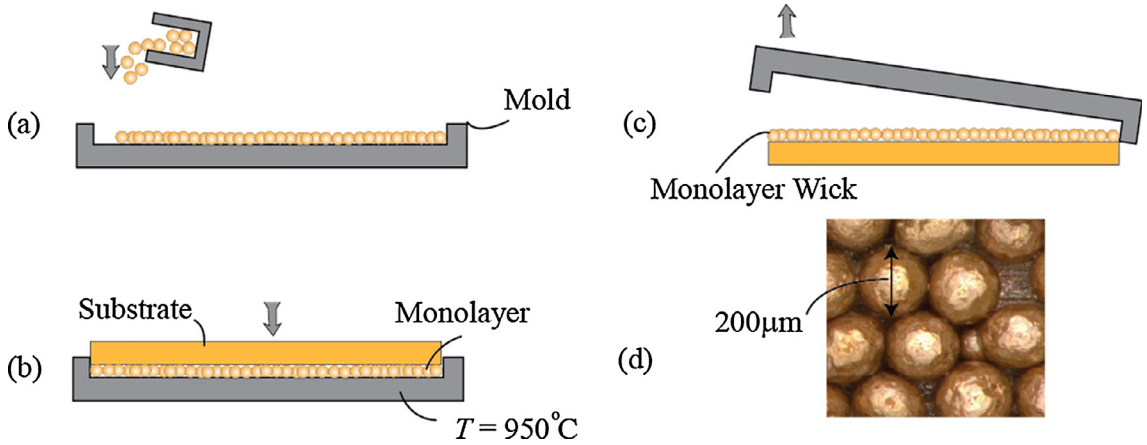

Fig. 2. Monolayer wick (Design B) sintered on the copper disk substrate using 200 μm copper particles. (a) Particles were poured in the mold, and the spread uniformly, (b) the substrate was aligned on the top with a small mechanical pressure, (c) the wick was released from the mold. (d) Fabricated monolayer wick image is also shown.

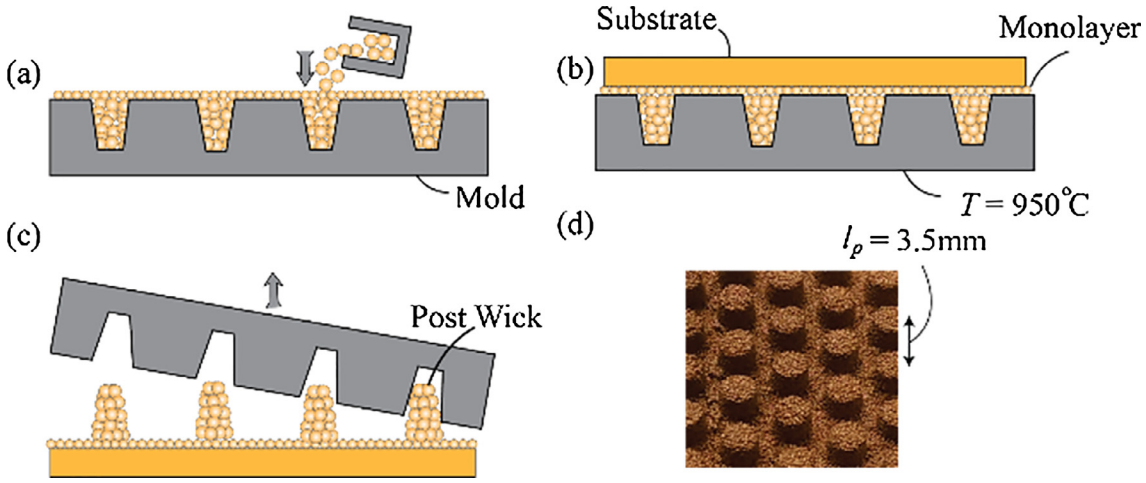

Fig. 3. A schematic of fabrication process of the columnar posts wick using a two-step sintering process. (a) Copper particles filled cavities of the first mold (posts); (b) monolayer particles packed over the mold, and the copper substrate placed on the top for the sintering process; (c) the first mold is removed and monolayer-posts-substrate is released; and (d) image of the fabricated wick with the pitch distance, l_p, also shown.

thermal contact resistance, and then these were mechanically in a good contact by compressing through the edge using screws. The different types of wicks such as monolayer wick (only), the columnar posts wick with the monolayer wick, and mushroom wick, were soldered with the copper base. The sample-attached copper base was placed at the bottom of the glass container. The *n*-pentane was used for the liquid pool as a working fluid. This allows not only for low saturation temperature, only 36.5 °C, which reduces the heat losses from the heater, but also for the CHF with a sufficiently large surface area for a minimal size (edge) effect. A cylindrical Teflon with O-rings was placed between the glass container and copper base to prevent from liquid leak. The Pyrex glass ring was placed around the boiling area to minimize the edge effect during the boiling. The condenser section was made of a copper coil and the cold water was used as the coolant. The whole condensation-evaporation setup was protected by a plastic cap to minimize vapor escape. Also, a flexible band heater was used to maintain the saturation temperature in the pool. The input power was controlled by variable voltage controllers for the desired heating power until it reached out CHF.

Several T-type thermocouples read the heater block temperature during the test. Two thermocouples were installed in the copper base separated 2.05 cm apart, with one installed only 4.5 mm from the boiling surface. Using these two temperatures, the heat flux was calculated by the Fourier law assuming one-dimensional heat flow. For the boiling surface temperature, T_s, was found by extrapolating these two temperatures. Another thermocouple was installed to monitor the temperature of the main copper heater. Also, the liquid temperature was measured at the boiling surface and the difference was used as the superheat. Tests were conducted increasing the input voltage to the heaters by small amounts in order to reach to a higher heat rate and keeping that until reaching a steady temperature. Steady state is defined when temperatures change $< \pm 0.5$ °C, over 5 min. This process continued until reaching to the total dry-out of the copper surface, where the significant superheat (~13–15 °C/min) increase was observed. Experiments were conducted at atmospheric pressure. Also, all the experimental results were reproduced by repeating at least two times for all cases, and the maximum differences were 4% in CHF and 8.5% in the wick superheat at given heat flux.

3.3. Uncertainty analyses

To assess the uncertainty in the measurements, the Kline and McClintock method is applied [72], as we have used before [73]. The uncertainty in the temperature and length measurements are estimated as ± 0.5 °C and 0.05 cm, respectively, and the property uncertainty is assumed as ± 0.5%. Then the uncertainty in heat flux is

$$U_q = q\left[\left(\frac{U_k}{k_s}\right)^2 + \left(\frac{U_{T_1}}{\Delta T}\right)^2 + \left(\frac{U_{T_3}}{\Delta T}\right)^2 + \left(\frac{U_{x1}}{\Delta x}\right)^2 + \left(\frac{U_{x2}}{\Delta x}\right)^2\right]^{0.5}. \quad (3)$$

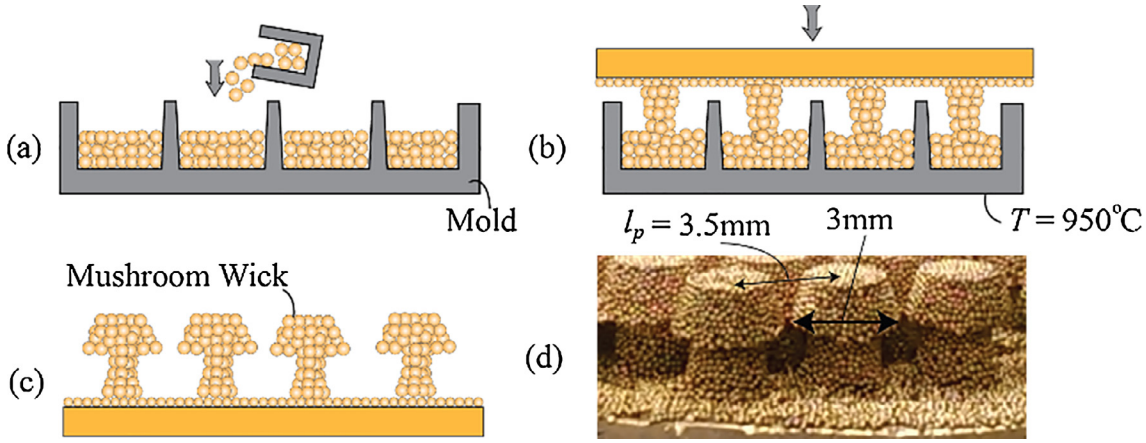

Fig. 4. A schematic of fabrication process on the mushroom wick (Design D) using a two-step sintering process. (a) Mushroom cap particles were poured in the second mold, (b) the columnar posts wick (Design C) was aligned on the top with a small mechanical pressure; (c) the mushroom posts wick was released from the second mold. (d) Fabricated mushroom posts wick with the pitch distance, l_p, also shown.

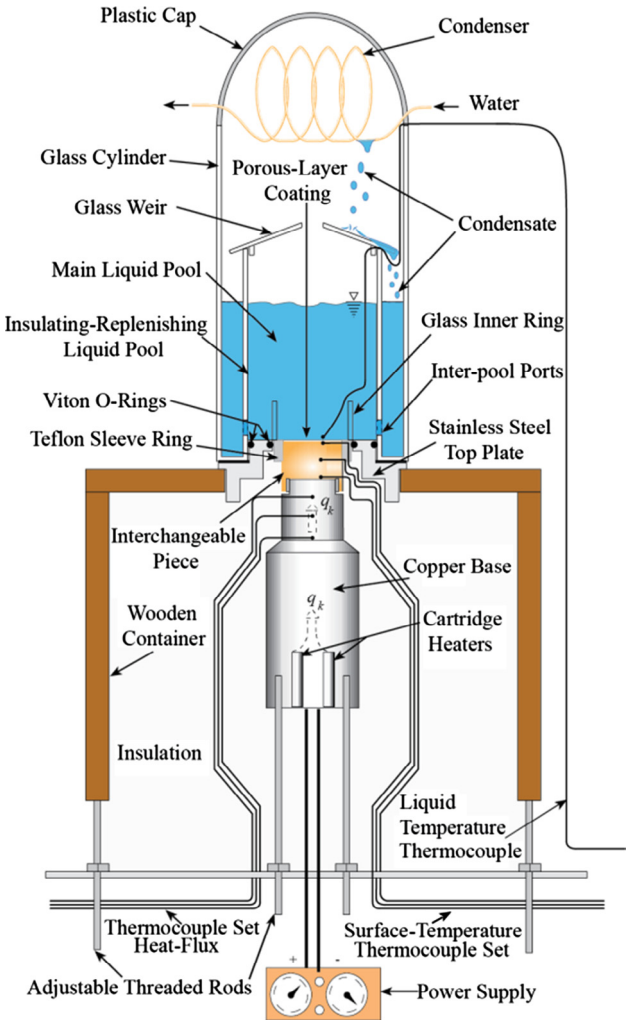

Fig. 5. A schematic of pool boiling setup, with heater, condenser, working fluid, and thermocouples.

The CHF uncertainty becomes

$$\frac{U_q}{q} = \left[(0.005)^2 + 2\left(\frac{0.5\ ^\circ\text{C}}{18\ ^\circ\text{C}}\right)^2 + 2\left(\frac{0.05\ \text{cm}}{2.05\ \text{cm}}\right)^2\right]^{0.5} \times 100 = 5.25\%$$

Similarly, the uncertainty for the surface-temperature measurement is

$$U_T = T\left[\left(\frac{U_k}{k_s}\right)^2 + \left(\frac{U_q}{q}\right)^2 + \left(\frac{U_{T_1}}{\Delta T}\right)^2 + \left(\frac{U_{x_1}}{\Delta x}\right)^2\right]^{0.5}. \quad (4)$$

The CHF temperature uncertainty is

$$\frac{U_T}{T} = \left[(0.005)^2 + (0.0525)^2 + \left(\frac{0.5\ ^\circ\text{C}}{5.7\ ^\circ\text{C}}\right)^2 + \left(\frac{0.05\ \text{cm}}{0.65\ \text{cm}}\right)^2\right]^{0.5} \times 100 = 12.8\%$$

The above uncertainties are used in the heat flux results discussed below.

4. Results and discussion

4.1. Plain surface

To validate experiments, the heat flux up to CHF was measured as a function of the superheat for the plain surface (polished, non-oxidized copper surface), as shown in Fig. 6. The average measured CHF was $q_{CHF} = 29 \pm 1.5\ \text{W/cm}^2$ from two separate experiments, and these reproducible results reasonably agree with the prediction using Eq. (1), $q_{CHF,Z} = 24.5\ \text{W/cm}^2$ [7] and $q_{CHF,R} = 31.7\ \text{W/cm}^2$ using Rohsenow correlation [74]. The oxidized plain surface results are compared with non-oxidized surface, showing a minimal difference. The results using the oxidized plain surface are used as a reference for comparisons with the coated surfaces, since the wicks are oxidized under exposure to air. Similar trends in the HTC have been found for other surface treatment conditions, and the predicted result using the coefficients for emergy polished surface [75,76] are shown in Fig. 6. In fact, a discrepancy between the predicted and experimental results may be caused by the different surface treatment.

4.2. Monolayer wick

Fig. 7 shows the pool boiling performance for the monolayer, having $q_{CHF} = 34.8 \pm 1.8\ \text{W/cm}^2$, which is 20% higher than that of the plain surface. This enhancement is related to the possible decrease in the hydrodynamic instability wavelength using the uniform porous wick [23]. However, this enhancement is smaller than the multiple-layer uniform wick which gives $q_{CHF} = 48\ \text{W/cm}^2$ [51], since it reduces the hydrodynamic instability wavelength more effectively than the monolayer wick [23]. The monolayer wick also reduces the superheat at given heat flux compared to the plain surface by increasing the HTC, and this is related to the increased effective thermal conductivity of the monolayer wick, etc. [35]. The further superheat reduction can be made with multiple-layer uniform wick, and this is related to enhanced effective thermal conductivity and/or the increased evaporation surface area compared to the monolayer wick [35,51,71,77].

The pool boiling heat transfer of the monolayer wick without columnar or mushroom posts wick shows the marginal improvements compared to the plain surface, but the role of the monolayer wick assisted by the columnar or mushroom posts is crucial to reduce the superheat, especially at high heat flux as discussed below.

4.3. Monolayer and columnar posts wick

To further enhance the CHF, the columnar posts plus the monolayer wicks are employed to actively control the hydrodynamic instability wavelength, with $l_p = \lambda_m = 3.5$ and 1 mm, through the post pitch, and

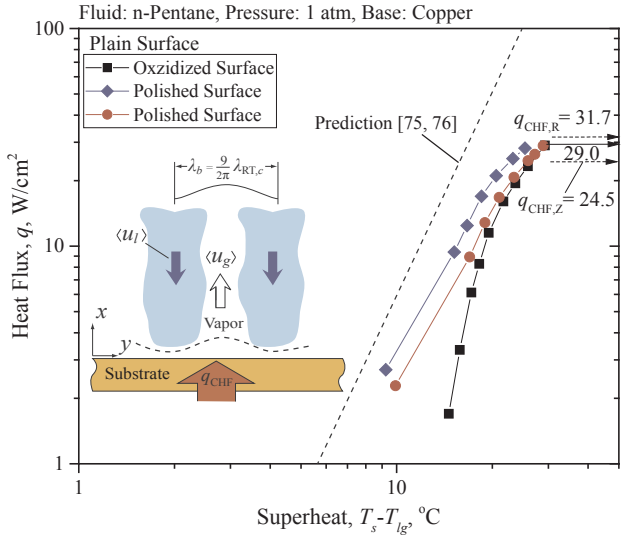

Fig. 6. Variations of the measured heat flux as a function of the superheat for the plain surface. The inset is the pool boiling hydrodynamic instability analysis leading to the Zuber CHF, $q_{CHF,Z}$ [Eq. (1)]. The predicted CHF using Rohsenow correlation, $q_{CHF,R}$ [74], and the Rohsenow superheat correlation results with coefficients for emergy polish surface [75,76] are also shown.

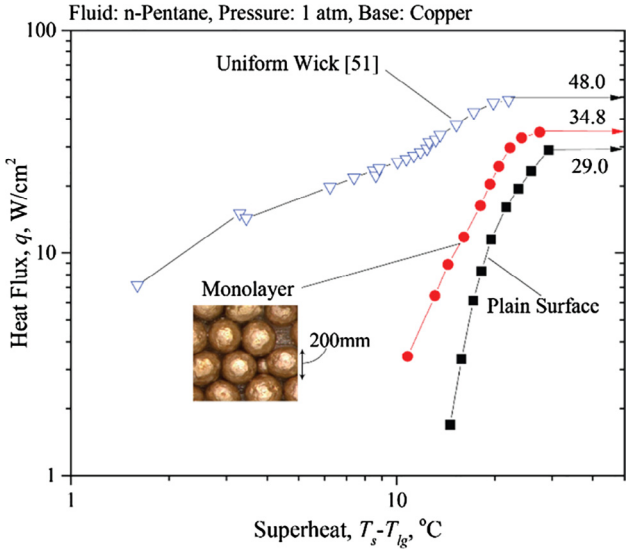

Fig. 7. Variations of measured heat flux with respect to the wick superheat for the monolayer and plain surface. The measured heat flux for the uniform coating wick is also shown [51]. The CHF for all cases are also marked.

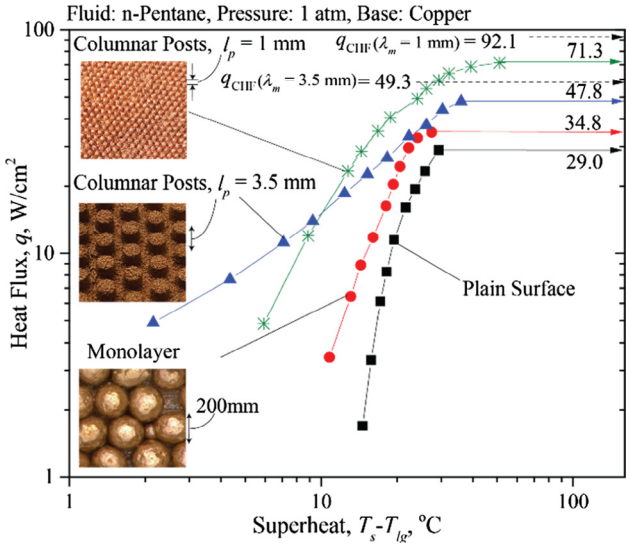

Fig. 8. Variations of measured heat flux as a function of the wick superheat for the monolayer, columnar posts wick, and plain surface. The CHF for all the tests are also marked.

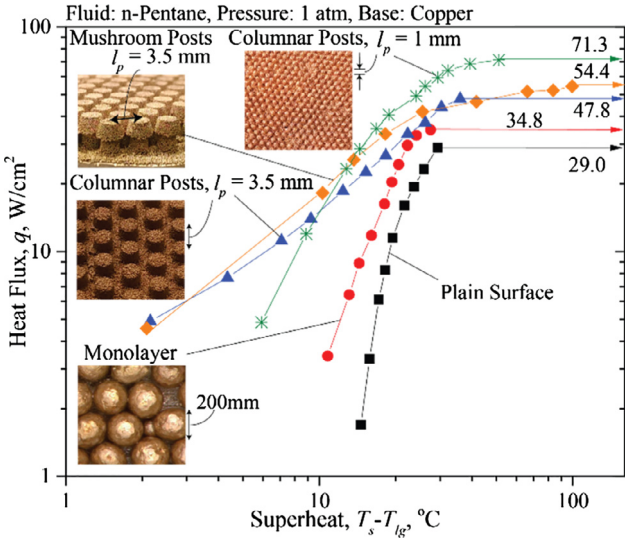

Fig. 9. Variations of measured heat flux as a function of the wick superheat for the monolayer, columnar and mushroom posts wicks (including images), and plain surface. The CHF for all the tests are also marked.

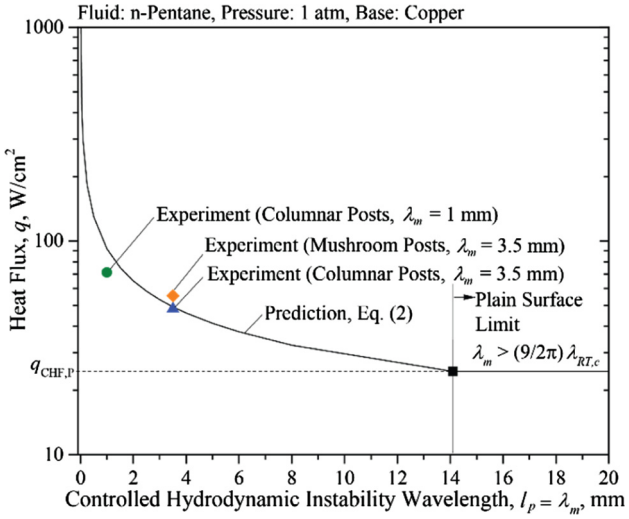

Fig. 10. Variations of the CHF hydrodynamic instability limit as a function instability wavelength, $l_p = \lambda_m$ (or post wick pitch). The measured CHF for the columnar and mushroom posts are also shown.

to reduce the wick superheat, similar to the previous study [51]. Fig. 8 shows the pool boiling performance for the columnar posts wick, compared to the monolayer wick and plain surface. The columnar posts with $l_p = \lambda_m = 3.5$ mm significantly reduces the superheat, especially at low heat flux compared to the monolayer only. The columnar posts wick significantly increases the overall thickness of the wick structure (~2 mm), which in turn is expected to increase the superheat due to larger conduction resistance, but the modulation decreases the superheat. This reduction is related to the thin monolayer wick with the vapor occupying in the space among the posts, i.e., the continuous vapor production over the monolayer wick surface compared to the poor, sporadic vapor production over the monolayer wick without posts wick. This reduction is nearly similar to that of the uniform 3–4-layer thick wick (0.6–0.8 mm) [51], as shown in Fig. 7. The CHF of the columnar posts wick also increases to $q_{CHF} = 47.8 \pm 2.5\ W/cm^2$ (65% enhancement compared to that of the plain surface) at larger superheat than that of the monolayer, i.e., delayed surface liquid dryout due to the increased liquid supply through the columnar posts.

The measured q_{CHF} reasonably agrees with the prediction using Eq. (2) with $l_p = \lambda_m = 3.5$ mm, showing the hydrodynamic instability control of the CHF. The hydrodynamic-instability-controlled CHF is further supported by the experimental observation using smaller pitch, i.e., $l_p = \lambda_m = 1$ mm. The measured q_{CHF} increases up to $71.3 \pm 3.7\ W/cm^2$, which is 2.5 times higher than that of the plain surface. This observed CHF is lower than the predicted CHF by Eq. (2), $q_{CHF} = 92.1\ W/cm^2$, and this can be due to defective structure [current fabrication limitation for the small pitch posts (the monolayer and posts partially peel off from the substrate when removing the mold after sintering)]. The defective structure also causes larger superheat at low heat flux and also near CHF, compared to the columnar posts wick with $\lambda_m = 3.5$ mm. The results show a reasonable trend from the prediction, i.e., the reduced hydrodynamic instability wavelength enhances the CHF. Also, the columnar posts with $l_p = \lambda_m = 1$ mm further reduce the wick superheat by increasing the HTC, especially at high heat flux regime. This may be related to the smaller pitch actively reducing the bubble sizes at departure and/or increased departure frequency,

however, the exact enhancement mechanism can be assisted by direct observation using high-speed visualization.

4.4. Monolayer and mushroom posts wick

For the mushroom posts wick, the measured heat flux as a function of the wick superheat is shown in Fig. 9, with the results similar to the columnar posts wick up to $q \sim 50\,W/cm^2$. The measured CHF using the mushroom posts wick is $q_{CHF} = 54.4 \pm 2.8\,W/cm^2$, which is the increase of 14% compared to the columnar, $q_{CHF} = 47.8\,W/cm^2$ with the expense of a larger superheat, i.e., $\Delta T = 80\,^{\circ}C$. The heat flux and superheat for $q < 50\,W/cm^2$ are very similar for the mushroom and columnar, but the mushroom cap significantly delays the surface dryout to superheat of 80 °C with a moderate CHF improvement. Thus, the mushroom pitch controls the hydrodynamic instability wavelength, i.e., $l_p = \lambda_m = 3.5\,mm$ in Eq. (2), the predicted CHF is $q_{CHF} = 49.3\,W/cm^2$, which reasonably agrees with the experimental results. The larger superheat at the CHF may be attributed to partial dryout in the monolayer, with enhanced liquid supply by the mushroom cap [61,64]. This larger superheat may be also related vapor escape in presence of the mushroom cap, and a high-speed visualization may provide an insight into this. In fact, the mushroom posts can be considered extended surface (3-D fins), however, this effect is rather minor compared to the hydrodynamic-instability controlled CHF [51].

To summarize, the measured CHF of the columnar and mushroom posts wick as a function of the pitch distance of the posts, i.e., active control of the hydrodynamic instability wavelength through the post wick pitch λ_m, are shown in Fig. 10. These experimental results are also compared with the prediction of Eq. (2), showing reasonable agreements, and this indicates that the hydrodynamic instability controls the CHF [51]. For the plain surface, the associated critical (largest disturbance) Rayleigh-Taylor instability wavelength $\lambda_{RT,c} = 2\pi\{\sigma/[g(\rho_l - \rho_g)]\}^{1/2}$, and the hydrodynamic instability wavelength for the *n*-pentane is $\lambda_m = (9/2\pi)\lambda_{RT,c} = 14\,mm$ [51,78]. This results in $q_{CHF} = 24.5\,W/cm^2$. The CHF increases by actively controlling the hydrodynamic instability wavelength using the columnar and mushroom posts along with the monolayer wick, i.e., $l_p = \lambda_m$.

The multilevel modulated wicks also enhance the HTC by assisting the liquid supply to the heated surface and favorably controlling the bubbles. Further modulation of the post and mushroom structures, effectively assists the liquid supply to the heated surface and favorably controls the departure bubble size and departure frequency leading to the enhanced HTC.

5. Conclusions

The multilevel modulated wick is employed to successfully demonstrate the simultaneous CHF and HTC enhancements. We find that the liquid-filled-monolayer significantly reduces the superheat by reducing the effective thermal conduction path, while the columnar posts actively modulates the critical hydrodynamic instability wavelength to enhance the CHF. It is observed that the monolayer wick improves the CHF by 20%, and the columnar and mushroom posts enhance the CHF by 65% and 87%, respectively, compared to the plain surface. These enhancements are achieved by actively reducing the hydrodynamic instability wavelength down to $\lambda_m = 3.5\,mm$, through the columnar posts for liquid supply path. The CHF further enhances up to 2.5 times compared to the plain surface, by further reducing the hydrodynamic instability wavelength λ_m down to 1 mm. Although the performance of the mushroom was similar to that of the columnar posts wick in the low heat flux (or low superheat) regime, the mushroom wick significantly delays the complete surface dryout by the continuous liquid supply through the mushroom cap, i.e., it allows for doubling the wick superheat at CHF compared to that of the columnar posts (no mushroom cap).

Acknowledgements

This work is financially supported by the University Research/Creative Projects (URCA) and start-up fund from Wichita State University. MK is thankful for financial support by the National Science Foundation (NSF), Thermal Transport and Processes Program (Award No. CBET-1623572).

References

[1] B. Agostini, M. Fabbri, J.E. Park, L. Wojtan, J.R. Thome, B. Michel, State of the art of high heat flux cooling technologies, Heat Transfer Eng. 28 (4) (2007) 258–281.
[2] R.C. Chu, R.E. Simons, M.J. Ellsworth, R.R. Schmidt, V. Cozzolino, Review of cooling technologies for computer products, IEEE Trans. Dev. Mater. Reliab. 4 (4) (2004) 568–585.
[3] I. Mudawar, T. Anderson, Optimization of enhanced surfaces for high flux chip cooling by pool boiling, J. Electron. Packag. 115 (1) (1993) 89–100.
[4] Z.J. Zuo, M.T. North, K.L. Wert, High heat flux heat pipe mechanism for cooling of electronics, IEEE Trans. Compon. Packag. Technol. 24 (2) (2001) 220–225.
[5] H.N. Chaudhry, B.R. Hughes, S.A. Ghani, A review of heat pipe systems for heat recovery and renewable energy applications, Renew. Sustain. Energy Rev. 16 (4) (2012) 2249–2259.
[6] R.T. Lahey, F.J. Moody, S. American Nuclear, R. United States. Energy, A. Development, The Thermal Hydraulics of a Boiling Water Nuclear Reactor, The Society, [Hinsdale, Ill.], 1977.
[7] N. Zuber, Hydrodynamic Aspects of Boiling Heat Transfer (Thesis), California. Univ., Los Angeles; and Ramo-Wooldridge Corp., Los Angeles, 1959.
[8] H.M. Kurihara, J.E. Myers, The effects of superheat and surface roughness on boiling coefficients, AIChE J. 6 (1) (1960) 83–91.
[9] W. Nakayama, T. Daikoku, T. Nakajima, Effects of pore diameters and system pressure on saturated pool nucleate boiling heat transfer from porous surfaces, J. Heat Transfer 104 (2) (1982) 286–291.
[10] R.L. Webb, N.-H. Kim, Principle of Enhanced Heat Transfer, John Wiley and Sons, New York, 1994.
[11] J. Wang, I. Catton, Enhanced evaporation heat transfer in triangular grooves covered with a thin fine porous layer, Appl. Therm. Eng. 21 (17) (2001) 1721–1737.
[12] S.W. Ahmad, T.G. Karayiannis, D.B.R. Kenning, A. Luke, Compound effect of EHD and surface roughness in pool boiling and CHF with R-123, Appl. Therm. Eng. 31 (11) (2011) 1994–2003.
[13] A.E. Bergles, M.C. Chyu, Characteristics of nucleate pool boiling from porous metallic coatings, J. Heat Transfer 104 (2) (1982) 279–285.
[14] A.K. Das, P.K. Das, P. Saha, Performance of different structured surfaces in nucleate pool boiling, Appl. Therm. Eng. 29 (17) (2009) 3643–3653.
[15] C.M. Patil, S.G. Kandlikar, Pool boiling enhancement through microporous coatings selectively electrodeposited on fin tops of open microchannels, Int. J. Heat Mass Transfer 79 (2014) 816–828.
[16] N.K. Choon, A. Chakraborty, S.M. Aye, W. Xiaolin, New pool boiling data for water with copper-foam metal at sub-atmospheric pressures: experiments and correlation, Appl. Therm. Eng. 26 (11) (2006) 1286–1290.
[17] L.W. Jin, K.C. Leong, I. Pranoto, Saturated pool boiling heat transfer from highly conductive graphite foams, Appl. Therm. Eng. 31 (14) (2011) 2685–2693.
[18] I. Pranoto, K.C. Leong, L.W. Jin, The role of graphite foam pore structure on saturated pool boiling enhancement, Appl. Therm. Eng. 42 (2012) 163–172.
[19] W. Nakayama, T. Daikoku, H. Kuwahara, T. Nakajima, Dynamic model of enhanced boiling heat transfer on porous surfaces—Part I: experimental investigation, J. Heat Transfer 102 (3) (1980) 445–450.
[20] J.P. O'Connor, S.M. You, A painting technique to enhance pool boiling heat transfer in saturated FC-72, J. Heat Transfer 117 (2) (1995) 387–393.
[21] K. Rainey, S. You, Pool boiling heat transfer from plain and microporous, square pin-finned surfaces in saturated FC-72, J. Heat Transfer 122 (3) (2000) 509–516.
[22] J. Han Kim, A. Gurung, M. Amaya, S. Muk Kwark, S.M. You, Microporous coatings to maximize pool boiling heat transfer of saturated R-123 and water, J. Heat Transfer 137 (8) (2015) 081501-081501-081507.
[23] G.-S. Hwang, M. Kaviany, Critical heat flux in thin, uniform particle coatings, Int. J. Heat Mass Transfer 49 (5) (2006) 844–849.
[24] A.M. Gheitaghy, H. Saffari, D. Ghasimi, A. Ghasemi, Effect of electrolyte temperature on porous electrodeposited copper for pool boiling enhancement, Appl. Therm. Eng. 113 (2017) 1097–1106.
[25] Y.-W. Lu, S.G. Kandlikar, Nanoscale surface modification techniques for pool boiling enhancement—a critical review and future directions, Heat Transfer Eng. 32 (10) (2011) 827–842.
[26] H.J. Cho, D.J. Preston, Y. Zhu, E.N. Wang, Nanoengineered materials for liquid–vapour phase-change heat transfer, Nat. Rev. Mater. 2 (2016) 16092.
[27] N.S. Dhillon, J. Buongiorno, K.K. Varanasi, Critical heat flux maxima during boiling crisis on textured surfaces, Nat. Commun. 6 (2015).
[28] X. Zheng, C.W. Park, Experimental study of the sintered multi-walled carbon nanotube/copper microstructures for boiling heat transfer, Appl. Therm. Eng. 86 (2015) 14–26.
[29] R. Ranjan, S.V. Garimella, J.Y. Murthy, K. Yazawa, Assessment of nanostructured capillary wicks for passive two-phase heat transport, Nanoscale Microscale Thermophys. Eng. 15 (3) (2011) 179–194.
[30] I.L. Pioro, W. Rohsenow, S.S. Doerffer, Nucleate pool-boiling heat transfer. I: Review of parametric effects of boiling surface, Int. J. Heat Mass Transfer 47 (23)

(2004) 5033–5044.
[31] H. Honda, J.J. Wei, Enhanced boiling heat transfer from electronic components by use of surface microstructures, Exp. Therm. Fluid Sci. 28 (2) (2004) 159–169.
[32] K. Nishikawa, T. Ito, K. Tanaka, Enhanced heat transfer by nucleate boiling on a sintered metal layer, Heat Transfer-Jpn. Res. 8 (2) (1979) 65–81.
[33] J.Y. Chang, S.M. You, Enhanced boiling heat transfer from microporous surfaces: effects of a coating composition and method, Int. J. Heat Mass Transfer 40 (18) (1997) 4449–4460.
[34] V.I. Borzenko, S.P. Malyshenko, Mechanisms of phase exchange under conditions of boiling on surfaces with porous coatings, High Temp. 39 (5) (2001) 714–721.
[35] J.H. Kim, K.N. Rainey, S.M. You, J.Y. Pak, Mechanism of nucleate boiling heat transfer enhancement from microporous surfaces in saturated FC-72, J. Heat Transfer 124 (3) (2002) 500–506.
[36] C. Li, G.P. Peterson, Y. Wang, Evaporation/boiling in thin capillary wicks (I)—wick thickness effects, J. Heat Transfer 128 (12) (2006) 1312–1319.
[37] C. Li, G.P. Peterson, Evaporation/boiling in thin capillary wicks (II)—effects of volumetric porosity and mesh size, J. Heat Transfer 128 (12) (2006) 1320–1328.
[38] C. Li, G.P. Peterson, Parametric study of pool boiling on horizontal highly conductive microporous coated surfaces, J. Heat Transfer 129 (11) (2007) 1465–1475.
[39] S. Launay, A.G. Fedorov, Y. Joshi, A. Cao, P.M. Ajayan, Hybrid micro-nano structured thermal interfaces for pool boiling heat transfer enhancement, Microelectron. J. 37 (11) (2006) 1158–1164.
[40] R. Furberg, B. Palm, Boiling heat transfer on a dendritic and micro-porous surface in R134a and FC-72, Appl. Therm. Eng. 31 (16) (2011) 3595–3603.
[41] E.J.T. Pialago, O.K. Kwon, C.W. Park, Nucleate boiling heat transfer of R134a on cold sprayed CNT–Cu composite coatings, Appl. Therm. Eng. 56 (1) (2013) 112–119.
[42] Z.G. Xu, C.Y. Zhao, Enhanced boiling heat transfer by gradient porous metals in saturated pure water and surfactant solutions, Appl. Therm. Eng. 100 (2016) 68–77.
[43] Y. Sun, G. Chen, S. Zhang, Y. Tang, J. Zeng, W. Yuan, Pool boiling performance and bubble dynamics on microgrooved surfaces with reentrant cavities, Appl. Therm. Eng. 125 (2017) 432–442.
[44] N.-H. Kim, K.-K. Choi, Nucleate pool boiling on structured enhanced tubes having pores with connecting gaps, Int. J. Heat Mass Transfer 44 (1) (2001) 17–28.
[45] D. Cooke, S.G. Kandlikar, Effect of open microchannel geometry on pool boiling enhancement, Int. J. Heat Mass Transfer 55 (4) (2012) 1004–1013.
[46] S.G. Kandlikar, Controlling bubble motion over heated surface through evaporation momentum force to enhance pool boiling heat transfer, Appl. Phys. Lett. 102 (5) (2013) 051611.
[47] C.M. Kruse, T. Anderson, C. Wilson, C. Zuhlke, D. Alexander, G. Gogos, S. Ndao, Enhanced pool-boiling heat transfer and critical heat flux on femtosecond laser processed stainless steel surfaces, Int. J. Heat Mass Transfer 82 (2015) 109–116.
[48] A. Jaikumar, S.G. Kandlikar, Ultra-high pool boiling performance and effect of channel width with selectively coated open microchannels, Int. J. Heat Mass Transfer 95 (2016) 795–805.
[49] N.S. Dhillon, J. Buongiorno, K.K. Varanasi, Critical heat flux maxima during boiling crisis on textured surfaces, Nat. Commun. 6 (2015) 8247.
[50] G. Hwang, C. Park, M. Kaviany, High-heat-flux distributed capillary artery evaporators, in: K. Vafai (Ed.), Handbook of Porous Media, CRC Press, third ed., 2015, pp. 597–630.
[51] S.G. Liter, M. Kaviany, Pool-boiling CHF enhancement by modulated porous-layer coating: theory and experiment, Int. J. Heat Mass Transfer 44 (22) (2001) 4287–4311.
[52] D. Min, G. Hwang, Y. Usta, O. Cora, M. Koc, M. Kaviany, 2-D and 3-D modulated porous coatings for enhanced pool boiling, Int. J. Heat Mass Transfer 52 (11–12) (2009) 2607–2613.
[53] C. Li, G.P. Peterson, Experimental study of enhanced nucleate boiling heat transfer on uniform and modulated porous structures, Front. Heat Mass Transfer (FHMT) 1 (2) (2010) 023007.
[54] Z.G. Xu, Z.G. Qu, C.Y. Zhao, W.Q. Tao, Pool boiling heat transfer on open-celled metallic foam sintered surface under saturation condition, Int. J. Heat Mass Transfer 54 (17) (2011) 3856–3867.
[55] Z.G. Qu, Z.G. Xu, C.Y. Zhao, W.Q. Tao, Experimental study of pool boiling heat transfer on horizontal metallic foam surface with crossing and single-directional V-shaped groove in saturated water, Int. J. Multiph. Flow 41 (2012) 44–55.
[56] A. Jaikumar, S.G. Kandlikar, Enhanced pool boiling for electronics cooling using porous fin tops on open microchannels with FC-87, Appl. Therm. Eng. 91 (2015) 426–433.
[57] L. Bai, L. Zhang, J. Guo, G. Lin, X. Bu, D. Wen, Evaporation/boiling heat transfer characteristics in an artery porous structure, Appl. Therm. Eng. 104 (2016) 587–595.
[58] Y. Tang, J. Zeng, S. Zhang, C. Chen, J. Chen, Effect of structural parameters on pool boiling heat transfer for porous interconnected microchannel nets, Int. J. Heat Mass Transfer 93 (2016) 906–917.
[59] G. Hwang, M. Kaviany, W. Anderson, J. Zuo, Modulated wick heat pipe, Int. J. Heat Mass Transfer 50 (7) (2007) 1420–1434.
[60] Y.S. Ju, M. Kaviany, Y. Nam, S. Sharratt, G.S. Hwang, I. Catton, E. Fleming, P. Dussinger, Planar vapor chamber with hybrid evaporator wicks for the thermal management of high-heat-flux and high-power optoelectronic devices, Int. J. Heat Mass Transfer 60 (2013) 163–169.
[61] G.S. Hwang, E. Fleming, B. Carne, S. Sharratt, Y. Nam, P. Dussinger, Y.S. Ju, M. Kaviany, Multi-artery heat-pipe spreader: lateral liquid supply, Int. J. Heat Mass Transfer 54 (11–12) (2011) 2334–2340.
[62] G.S. Hwang, Y. Nam, E. Fleming, P. Dussinger, Y.S. Ju, M. Kaviany, Multi-artery heat pipe spreader: experiment, Int. J. Heat Mass Transfer 53 (13–14) (2010) 2662–2669.
[63] D. Min, G. Hwang, M. Kaviany, Multi-artery, heat-pipe spreader, Int. J. Heat Mass Transfer 52 (3) (2009) 629–635.
[64] M. Kim, M. Kaviany, Multi-artery heat-pipe spreader: monolayer-wick receding meniscus transitions and optimal performance, Int. J. Heat Mass Transfer 117 (2018) 1158–1168.
[65] M. Kim, M. Kaviany, Flow-boiling canopy wick for extreme heat transfer, Int. J. Heat Mass Transfer 117 (2018) 1158–1168.
[66] C. Ramaswamy, Y. Joshi, W. Nakayama, W. Johnson, Effects of varying geometrical parameters on boiling from microfabricated enhanced structures, J. Heat Transfer 125 (1) (2003) 103–109.
[67] J.A. Weibel, S.V. Garimella, M.T. North, Characterization of evaporation and boiling from sintered powder wicks fed by capillary action, Int. J. Heat Mass Transfer 53 (19) (2010) 4204–4215.
[68] J.Y. Chang, S.M. You, Heater orientation effects on pool boiling of micro-porous-enhanced surfaces in saturated FC-72, J. Heat Transfer 118 (4) (1996) 937–943.
[69] K.N. Rainey, S.M. You, G. Li, Flow boiling heat transfer from plain and microporous coated surfaces in subcooled FC-72, J. Heat Transfer 123 (5) (2001) 918–925.
[70] J.Y. Chang, S.M. You, Boiling heat transfer phenomena from microporous and porous surfaces in saturated FC-72, Int. J. Heat Mass Transfer 40 (18) (1997) 4437–4447.
[71] S.G. Liter, Pool-boiling Enhancement and Liquid Choking Limits within and Above a Modulated Porous-layer Coating, University of Michigan., 2000.
[72] S.J. Kline, F.A. McClintock, Describing uncertainties in single-sample experiments, Mech. Eng. 75 (1958) 3–8.
[73] S.G. Liter, Pool-boiling Enhancement and Liquid Choking Limits within and Above a Modulated Porous-layer Coating, University of Michigan, 2000.
[74] W.M. Rohsenow, P. Griffith, Correlation of maximum heat flux data for boiling of saturated liquids, Chem. Eng. Prog. 52 (1956) 47.
[75] W.M. Rohsenow, A method of correlating heat transfer data for surface boiling of liquids, Trans. Am. Soc. Mech. Eng. 74 (1952) 969–975.
[76] R.I. Vachon, G.H. Nix, G.E. Tanger, Evaluation of constants for the Rohsenow pool-boiling correlation, J. Heat Transfer 90 (2) (1968) 239–246.
[77] S. Sarangi, J.A. Weibel, S.V. Garimella, Effect of particle size on surface-coating enhancement of pool boiling heat transfer, Int. J. Heat Mass Transfer 81 (2015) 103–113.
[78] N. Zuber, Hydrodynamic Aspects of Boiling Heat Transfer (Ph.D. Thesis), University of California, Los Angeles, CA, 1959.